Transition from Nanodomains to Microdomains Induced by Exposure of Lipid Monolayers to Air

Oana Coban, Jesse Popov, Melanie Burger, Dusan Vobornik, and Linda J. Johnston

Steacie Institute for Molecular Sciences, National Research Council Canada, Ottawa, Canada K1A OR6

ABSTRACT   The morphology of monolayers prepared from ternary lipid mixtures that have coexisting fluid phases has been examined by atomic force microscopy for samples transferred to mica before and after exposure to air. Mixtures of 1,2-dioleoyl-*sn*-glycero-3-phosphocholine and cholesterol with either egg sphingomyelin or 1,2-dipalmitoyl-*sn*-glycero-3-phosphocholine were studied at several surface pressures. Both lipid mixtures have a combination of small islands and large microdomains at low surface pressure (5–10 mN/m) for monolayers deposited in either air or nitrogen. By contrast, monolayers have small interconnected nanodomains when deposited under nitrogen at 30 mN/m but mixtures of large microdomains and small nanodomains when transferred after exposure to air. These results are consistent with an earlier report that concluded that the formation of large domains at high surface pressures (>30 mN/m) for monolayers exposed to air is caused by lipid oxidation. However, the higher spatial resolution available with atomic force microscopy indicates that exposure of the monolayers to air leads to an increase in the size of preexisting nanodomains, rather than a change in the miscibility pressure. Examination of changes in surface morphology as a function of surface pressure demonstrate a gradual evolution in size and surface coverage for both nano- and microdomains, before formation of a network of interconnected nanodomains. Similar studies for binary mixtures in the absence of cholesterol indicate that lipid oxidation results in analogous changes in domain size for monolayers with coexisting gel and fluid phases. These results illustrate the importance of using techniques capable of probing the nanoscale organization of membranes.

INTRODUCTION

The organization of lipids in cell membranes has been the subject of extensive investigation over the last decade, with much attention focused on providing evidence for the existence and function of lipid rafts (1–4). Lipid rafts are dynamic membrane domains that are enriched in saturated lipids such as sphingomyelin (SM), glycosphingolipids, and cholesterol (Chol) and characterized by tight packing of lipid acyl chains but high mobility of the individual lipids. They are believed to exist in a liquid-ordered phase that is surrounded by the bulk fluid disordered membrane and are postulated to be involved in cellular processes such as signaling and membrane trafficking. Studies in natural membranes have resulted in many conflicting estimates of the size, stability, and protein and lipid composition of lipid rafts (5–8). The formation of domains has also been extensively studied in models such as vesicles and supported membranes that have provided much of our current understanding of the molecular interactions that determine membrane structure and function. Of particular relevance to the lipid raft hypothesis is the observation of coexisting liquid phases in model systems. Initial studies provided evidence for coexisting liquid-ordered and liquid-disordered phases in Chol/phospholipid mixtures (9,10). More recently coexisting liquid phases in ternary lipid mixtures have been visualized directly using fluorescence microscopy in giant vesicles (11–13) and sup-

ported membranes (14–16) and also using atomic force microscopy (AFM) for lipid monolayers and bilayers (17–21). Ternary lipid mixtures comprised of saturated SM, an unsaturated phosphatidylcholine, and Chol have now been extensively used to model the behavior of lipid rafts (7,13,22,23). Although they do reproduce the coexisting liquid phases postulated for raft domains in natural membranes, there are important differences. For example, in giant vesicles large micrometer-sized raft domains that extend through both leaflets of the bilayer are observed; these results mimic neither the small size (typically <200 nm) nor the asymmetry of lipid rafts in cellular membranes.

The use of supported membranes prepared from Langmuir monolayers is an attractive method for preparing supported bilayers for studies of domain formation because it allows for the fabrication of asymmetric bilayers (24). By contrast, the composition of the individual leaflets cannot be independently controlled for bilayers prepared by vesicle fusion. However, two recent studies have shown that the phase separation behavior of ternary lipid mixtures is dramatically modified by lipid oxidation when monolayers are prepared in air (25,26). For example, mixtures of 1:1 brain SM/1,2-dioleoyl-*sn*-glycero-3-phosphocholine (DOPC) with 20% Chol form large micron-sized domains of a liquid-ordered SM/Chol-rich phase below the miscibility transition pressure of 14.5 mN/m and a single homogeneous phase above this pressure in an argon environment. However, lateral heterogeneity on the micrometer scale is observed over a much wider range of surface pressure (up to 32 mN/m) for samples in air, an effect that is attributed to a large increase in the

miscibility transition pressure due to the formation of oxidized lipids for monolayers at the air-water interface (25). These studies have used dye-labeled lipids and conventional fluorescence microscopy to visualize phase coexistence in monolayers before and after oxidation. The method employed does not have the ability to resolve small closely spaced nanodomains, should they exist, on spatial scales below the diffraction limit (~300 nm).

The results for oxidation of lipid monolayers of ternary lipid mixtures that mimic rafts are consistent with earlier data on oxidation of monolayers containing unsaturated lipids or Chol in the presence of either oxygen or ozone (27–29). They also raise concerns as to the validity of literature data for raft membranes prepared using Langmuir monolayers (16). Nevertheless, the observation of phase separation for similar raft mixtures in bilayer membranes in vesicles is in contrast to the apparently homogeneous mixture observed for unoxidized monolayers. Although changes between the phase behavior of monolayers and bilayers may account for this difference, an alternate possibility is that the unoxidized monolayers show domains on a much smaller length scale. Such behavior has previously been observed by AFM for several supported monolayers (30,31) and bilayers (21,32,33). We have therefore examined the morphology of monolayers deposited under air and nitrogen using high resolution scanning probe microscopy techniques that can resolve domains on the nanometer scale. Herein we use AFM and near-field scanning optical microscopy (NSOM) to study the effects of air exposure on phase separation in monolayers prepared from two ternary lipid mixtures that have coexisting fluid phases and from the corresponding binary mixtures in the absence of Chol, which have coexisting gel and liquid-disordered phases. We conclude that there is an evolution from micrometer-sized to nanodomains with increasing surface pressure, illustrating the importance of using techniques that are capable of resolving membrane organization on the nanometer scale for studying domain formation in model membranes. We also report that air exposure promotes the formation of large microdomains from monolayers that have only nanodomains under nitrogen, effects that are postulated to be due to lipid oxidation and that indicate the importance of preventing oxidation in studies of phase separation in lipid monolayers.

MATERIALS AND METHODS

Materials

DOPC, egg sphingomyelin (ESM), 1,2-dipalmitoyl-*sn*-glycero-3-phosphocholine (DPPC), and Chol were obtained from Avanti Polar Lipids (Alabaster, AL). DOPC was purchased as a chloroform solution at a concentration of 10 mg/ml in ampoules sealed under nitrogen and was stored at −20°C. All other lipids were stored as lyophilized powders at −20°C. High-performance liquid chromatography grade chloroform and methanol were from ACP Chemicals (Quebec, Canada). Texas Red 1,2-dihexadecanoyl-*sn*-glycero-3-phosphoethanolamine, triethylammonium salt (Texas Red DHPE) was

purchased from Invitrogen Canada (Ontario, Canada). Dihydrocholesterol ((Dchol) 5α-cholestan-3β-ol) was obtained from Sigma (Ontario, Canada).

Monolayer preparation

Planar supported monolayers were prepared on a Langmuir-Blodgett trough (611 NIMA, Coventry, UK) using Milli-Q water as the subphase. To prevent oxidation, the trough was placed in a glove box (830-Compact Glove Box, Plas Labs, Lansing, MI) filled with nitrogen that ensured an inert environment for monolayer preparation. Fresh stock solutions of lipid were prepared in chloroform before each sample preparation. When DOPC was used for the lipid mixture a new ampoule was opened for each experiment. Lipid mixtures (ratios in mol %) were spread on the water surface at ~5 mN/m and allowed to equilibrate to a constant surface pressure upon solvent evaporation (2–5 min). The surface pressure was measured with a precision of 0.1 mN/m using a Wilhelmy balance. Monolayers were annealed by at least two compression/expansion cycles at 150 cm²/min and once again at 75 cm²/min. Monolayers were transferred to freshly cleaved, hydrophilic mica at a preset pressure by vertical deposition at a dipping speed of 2 mm/min. To prepare oxidized monolayers, the glove box was preequilibrated with air for at least 40 min and lipids were deposited on the trough at ~8 mN/m. Lipids were maintained at the air-water interface for 20–30 min. The barrier was then fully opened or until the surface pressure dropped below 1 mN/m and the monolayer was annealed according to the same compression/expansion cycle. Fluorescent lipid concentrations as high as 1 mol % were used to label the fluid phase without any significant change in the monolayer morphology.

The DOPC/ESM/Chol monolayers are very sensitive to traces of air. We find that it is impossible to obtain results similar to those in an inert environment by simply making monolayers as rapidly as possible in air and that it is crucial to thoroughly purge the glove box to remove air. By contrast, traces of air that are sufficient to cause oxidation of raft monolayers containing ESM have no effect on monolayer morphology for DPPC raft mixtures. This provides qualitative evidence that the DOPC/DPPC/Chol monolayers are less sensitive to oxidation. We determined the length of time that the inert environment inside the glove box could be maintained without additional purging by depositing a monolayer under nitrogen at 30 mN/m immediately after equilibration and solvent evaporation, a second one after the lipids were allowed to sit for 1 h at the nitrogen-water interface, and a third one after 2 h. The monolayers deposited immediately and 1 h later were indistinguishable but a small increase (<10%) in the domain size was observed for the monolayer deposited after 2 h (data not shown). This suggests that inside the glove box there may be sufficient residual oxygen to cause a slight increase in the domain sizes for long exposure times. To provide more evidence that the microdomains observed at low pressure are not the result of potential trace amounts of oxygen that can trigger lipid oxidation and reorganization we transferred a monolayer at 10 mN/m and subsequently a second one at 30 mN/m from the same lipid monolayer at the nitrogen-water interface. This experiment is performed within <1 h, a time window that gives no detectable change in the nanoscale monolayer morphology at high surface pressure. The resulting monolayers showed large domains at 10 mN/m and small interconnected domains at 30 mN/m, indicating that the large domains at 10 mN/m are not the result of lipid oxidation.

Scanning probe microscopy

Atomic force microscopy measurements were performed on a Multimode Nanoscope III (Digital Instruments, Santa Barbara, CA) in contact mode in air. The monolayer samples were scanned at constant force using a piezo-electric J scanner (maximum scan area 120 × 120 μm²) and soft cantilevers (~200 μm long) with integrated pyramidal tips (spring constant ~120 mN/m). Usually, regions ranging from 100 × 100 μm² to 5 × 5 μm² were imaged at a resolution of 512 × 512 pixels using a scan rate of 1 Hz. Differences in height between coexisting phases of the monolayers were

determined using the cross-section analysis routine of the DI software. The bearing analysis routine was used to construct histograms for measuring the fraction of the monolayer surface covered by domains.

Near-field scanning optical microscopy experiments were carried out on a combined AFM/NSOM microscope. The NSOM setup is based on a Digital Instruments Bioscope mounted on an inverted microscope (Axiovert 100 TV, Zeiss, Jena, Germany) using an Ar^+-Kr^+ ion laser (Innova 70 Spectrum; Coherent, Santa Clara, CA) as the excitation source. The laser light (488 nm) is delivered to the microscope via a single-mode fiber (Mitsubishi, Tokyo, Japan). The bent NSOM probe is fabricated from this optical fiber using a two-step chemical etching method followed by aluminum deposition and focused ion beam milling to produce the aperture. All experiments were performed with a tip aperture size of <100 nm and estimated spring constant of 100 N/m. A more detailed description of the probe fabrication and characterization is given elsewhere (34). A piezoelectric, two-dimensional scanning stage with feedback control (E-50100, Physick Instrumente, Karlsruhe, Germany) allows the sample to be scanned. Fluorescence is collected through an air objective (Ldplan-Neofluar, 63×, Korr, NA = 0.75, Zeiss), passed through an appropriate filter to remove residual excitation light (488 nm Notch filter; Kaiser Optical Systems, Ann Arbor, MI) and a bandpass filter (590DF35; Omega Optical, Brattleboro, VT) and detected by an avalanche photodiode (EG&G, SPCM-AQR-14, Perkin Elmer, Vaudreuil, Canada). Images were collected in tapping mode in air at a scan rate of typically 0.25 Hz and a resolution of 512 × 512 pixels.

Total internal reflection fluorescence microscopy

Diffraction-limited fluorescence measurements of supported monolayers were carried out on an objective-type inverted microscope (Olympus IX81; Olympus, Tokyo, Japan). The excitation source used for Texas Red DHPE is the 543-nm line of a He-Ne laser (Melles Griot, Carlsbad, CA). The laser beam is focused on the sample by means of an oil-immersion objective (PlanApo N, 60×, Korr, NA = 1.45, Olympus). The fluorescence light is collected through the same objective, passed through the appropriate filters (Ex, HQ560/55; Em, HQ645/75; BS, Q595LP; Chroma Technology, Brattleboro, VT) and focused onto a charge-coupled device camera (CoolSnap ES; Roper Scientific Photometrics, Tucson, AZ). Image acquisition is controlled using Image Pro 5.1 software. Images were collected at a resolution of 93 × 93 pixels, with 260 nm/pixel. No significant optical interference from the supporting mica substrate was observed.

RESULTS

The effects of air exposure on monolayer morphology have been examined by imaging monolayers of two ternary lipid mixtures that are frequently used to model lipid rafts. One of the mixtures contains ESM, the unsaturated lipid DOPC, and Chol. In the second mixture we replaced ESM with the saturated lipid DPPC. For comparison, we have also examined monolayers of the corresponding binary mixtures in the absence of Chol, and monolayers in which Chol is replaced by Dchol. Monolayers were deposited at low and high surface pressures (5 or 10 mN/m and 30 mN/m, respectively) in either a nitrogen or air atmosphere. These pressures were selected based on previous fluorescence microscopy studies demonstrating that monolayers had similar morphologies in air and argon atmosphere at surface pressures that were below the miscibility transition pressure as judged by the point at which large micrometer-sized domains disappear (25,26). The higher pressure is within the range (30–35 mN/m) that is considered appropriate for modeling a cellular mem-

brane (35,36). A combination of AFM and NSOM is used to confirm that topographic and fluorescence contrast give the same results. This provides a more direct comparison with earlier studies and ensures that the addition of up to 1% Texas Red-DPPE does not modify the phase separation behavior of the monolayers studied.

Monolayer morphology for ESM lipid mixtures

Representative AFM images for 1:1 DOPC/ESM with 20% Chol monolayers transferred to mica at surface pressures of 10 and 30 mN/m under nitrogen and in air are shown in Fig. 1. At 10 mN/m deposition pressure the monolayer shows micrometer size (~10–20 μm) raised domains and a few small islands surrounded by a lower phase. By analogy to earlier monolayer studies (17,20,30), the raised domains and islands are assigned to an ESM/Chol-rich phase, which is surrounded by a liquid-disordered DOPC-rich phase. Similar morphologies were obtained independent of whether the monolayer was under nitrogen (Fig. 1 A) or in air (Fig. 1 B). In both cases, the height difference between liquid-ordered and liquid-disordered phases was 0.9–1 nm. When monolayers were deposited at 30 mN/m, phase separation was still observed but there was a significant change in morphology for monolayers exposed to air before transfer. Small interconnected domains (~70–200 nm mean diameter) were observed in monolayers prepared under nitrogen (Fig. 1 C). The liquid-ordered phase was ~0.7 nm higher than the fluid phase. A monolayer exposed to air before deposition at 30 mN/m (Fig. 1 D) exhibits a similar morphology to monolayers deposited at 10 mN/m. This change in morphology from small interconnected to larger isolated domains was accompanied by a slight increase in the height difference between the two phases to 0.9–1 nm (see cross sections in Fig. 1 E and Table 1). At both surface pressures, monolayers deposited under air showed an increase of ~10% in the surface coverage for the raised domains (see histogram in Fig. 1 F and Table 1). Note that quantifying the surface coverage requires averaging data from histograms for multiple images in cases where there are relatively few large domains, as in Fig. 1 D.

The existence of microdomains and interconnected nanodomains in monolayers deposited under nitrogen at low and high pressure, respectively, has been confirmed in at least five individual experiments using different batches of lipids. Microdomains in monolayers transferred at low pressure were of similar size between repeat experiments and they were always surrounded by a variable number of small islands of ESM/Chol with sizes between 75 and 350 nm. We noted some variability in the shape of the microdomains ranging from elliptical domains with irregularly shaped or rounded edges to teardrop-shaped domains. The packing density and the interconnectivity between the nanodomains observed in monolayers deposited at high pressure also varied slightly between different experiments but the overall percolation
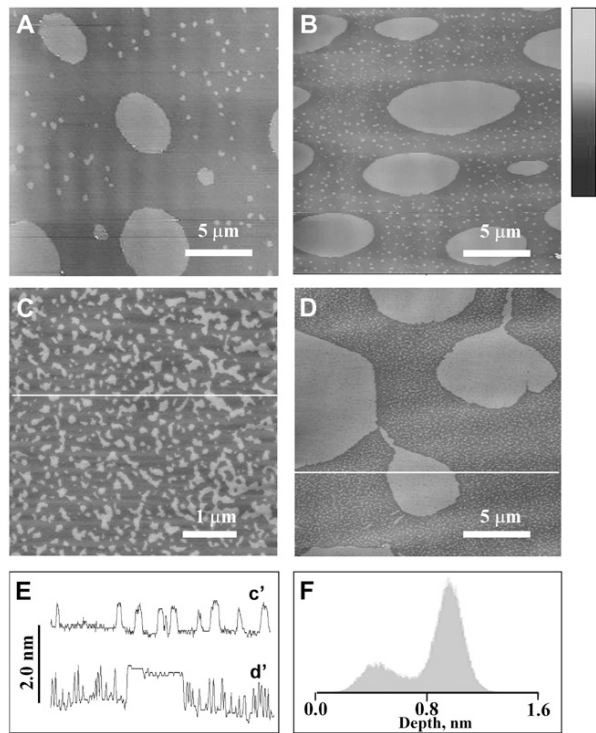
FIGURE 1 Effect of air exposure on monolayers of 1:1 DOPC/ESM with 20 mol % Chol. (*A* and *B*) Monolayers deposited at 10 mN/m under nitrogen and in air, respectively. (*C* and *D*) Monolayers transferred at 30 mN/m under nitrogen and in air, respectively. The *z*-scale is 10 nm for images *A*, *B*, and *D* and 5 nm for image *C*. Cross sections (*c'* and *d'*) for the lines indicated in images *C* and *D*, respectively, are shown in panel *E* displayed on the same length scale as the image. The histogram in panel *F* shows the height difference between domains and fluid phase for image *C*.

pattern was reproducible. In no case have we observed a homogeneous monolayer for the raft mixture. Similar changes in morphology as a function of air exposure before deposition were also observed for monolayers of ternary lipid mixtures in which ESM was replaced by either brain SM or palmitoyl SM.

TABLE 1 Height differences between domains and fluid phase and surface area covered by domains for binary and ternary lipid mixtures deposited under nitrogen and air

Lipid mixture	Surface pressure, mN/m	Height, nm (% coverage) Nitrogen	Height, nm (% coverage) Air
DOPC/ESM + 20% Chol	10	0.9–1 (28%)	0.9–1 (38%)
	30	0.7 (27%)	0.9–1 (40%)
DOPC/ESM	10	1.3–1.4	1.1–1.2
	30	0.9	1.2
DOPC/DPPC + 20% Chol	5	0.9–1	0.9–1
	30	0.7–0.8	0.7–0.8
DOPC/DPPC	10	1.1	1.1
	30	0.7–0.8	0.7–0.8
DOPC/DPPC + 20% Dchol	30	0.6–0.7 (28%)	0.7–0.8 (34%)

By contrast, exposure of dry monolayers on mica to air did not result in any detectable change in morphology for any of the samples studied.

Fig. 2 shows AFM images of 1:1 DOPC/ESM monolayers transferred at 10 mN/m and 30 mN/m under nitrogen (Fig. 2, *A* and *C*) and in air (Fig. 2, *B* and *D*). The morphology of DOPC/ESM monolayers transferred at 10 mN/m under nitrogen was dominated by small islands (200–250 nm) surrounded by a lower phase. The height difference between the two phases was 1.3–1.4 nm. Monolayers formed under air and transferred at 10 mN/m exhibited larger domains (1–3 μm) that were 1.1–1.2 nm taller than the surrounding fluid phase (Table 1). Further compression of the unoxidized lipid monolayer to 30 mN/m generated a mixture of small domains (200–300 nm) that are aligned to form parallel stripes across the sample and randomly distributed small islands (70–100 nm), both of which are ~0.9 nm higher than the surrounding fluid phase. Formation of stripes by alignment of circular or elliptical domains during monolayer transfer has been previously observed (31,37,38). Exposure of lipid monolayers to air before transfer at 30 mN/m led to formation of large domains (1–3 μm) in addition to the stripes of small aligned islands observed for samples deposited under nitrogen. The gel domains were ~1.2 nm taller than the fluid phase. At 10 mN/m, SM monolayers have coexisting liquid condensed and liquid expanded phases, whereas at 30 mN/m a single gel phase monolayer is obtained (39). Thus, we attribute the small domains obtained at 10 mN/m for the DOPC/ESM monolayer to condensed ESM domains
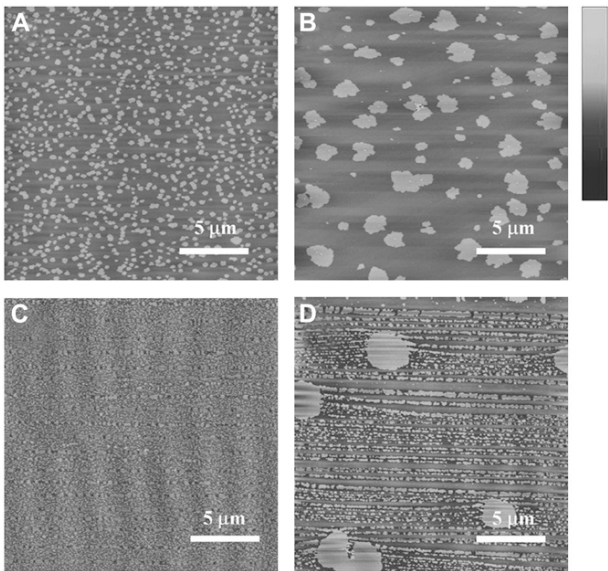

FIGURE 2 AFM images of 1:1 DOPC/ESM monolayers transferred to mica at 10 (*A* and *B*) and 30 mN/m (*C* and *D*). Monolayers shown in Fig. 2, *A* and *C*, were deposited under nitrogen whereas those shown in Fig. 2, *B* and *D*, were deposited in air. The *z*-scale is 10 nm for images *A* and *B* and 5 nm for images *C* and *D*.

surrounded by a lower, fluid DOPC/ESM phase. At 30 mN/m, gel phase ESM domains are surrounded by a fluid phase that is predominantly DOPC.

## Monolayer morphology for DPPC lipid mixtures

AFM images of 1:1 DOPC/DPPC monolayers containing 20% Chol deposited at two surface pressures in nitrogen and air are shown in Fig. 3. The effects of air versus nitrogen at the higher pressure are significant and are analogous to the results obtained for ternary lipid mixtures containing ESM. The small interconnected domains observed at 30 mN/m under nitrogen are replaced by large raised domains in air (Fig. 3, *C* and *D*). By contrast, monolayers deposited at 5 mN/m have mixtures of small and large domains that are similar under air and nitrogen (Fig. 3, *A* and *B*, respectively). The deposition pressure was lowered to 5 mN/m since the small interconnected domains were still observed at 10 mN/m for this mixture. There was no difference in height between domains and fluid phase after exposure to air (Table 1). An additional experiment was carried out to check that the effect of air on the monolayer morphology was irreversible. In this case a monolayer at 30 mN/m prepared under nitrogen was exposed to air for 30 min and then the air in the box was replaced by thoroughly purging with nitrogen. The monolayer deposited after reequilibration of the box with nitrogen showed large domains similar to the monolayer

prepared in air (see *inset* in Fig. 3 *D*). By contrast, a monolayer kept under nitrogen for the same length of time before deposition still showed small interconnected domains (data not shown).

Monolayers of binary mixtures of 1:1 DOPC/DPPC were also examined. Typical images for DOPC/DPPC monolayers transferred to mica at surface pressures of 10 and 30 mN/m under nitrogen and after exposure to air are shown in Fig. 4. For monolayers deposited at 10 mN/m under nitrogen, we observe large rounded domains (1–3 μm) that are ~1.1 nm higher than the surrounding matrix (Fig. 4 *A*). Monolayers deposited under air were not significantly different (Fig. 4 *B*). At 10 mN/m, DPPC is predominantly in a condensed phase so the domains are assigned to DPPC with a surrounding DOPC fluid phase. DOPC/DPPC monolayers transferred at 30 mN/m showed micrometer-size domains (5–15 μm) with a "flower-like" shape (Fig. 4 *C*) in addition to stripes formed by alignment of many small islands, similar to earlier studies for monolayers transferred at 37 mN/m (31). The height difference between the two phases was 0.7–0.8 nm. No significant change in the monolayer morphology or height difference between the two phases was observed upon exposure to air (Fig. 4 *D*).

Effect of surface pressure

The high spatial resolution of AFM allows the detection of coexisting phases in monolayers of 1:1 DOPC/ESM and 20% Chol deposited under nitrogen at a pressure as high as 30 mN/m. To investigate the change in morphology from
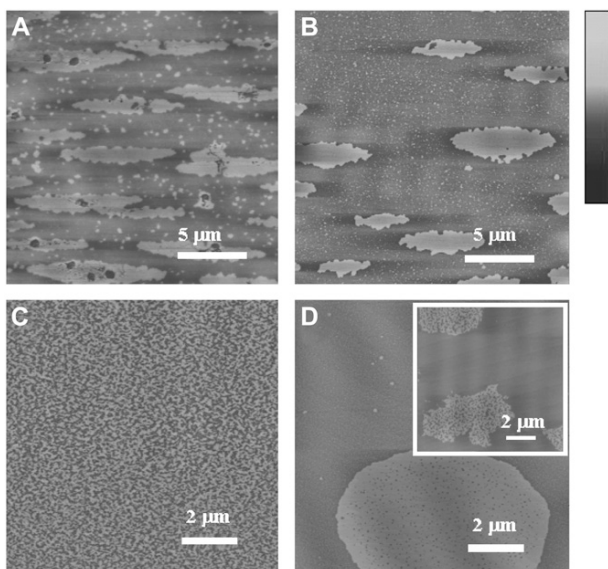
FIGURE 3 Effect of air exposure on supported monolayers of 1:1 DOPC/DPCC with 20 mol % Chol. (*A* and *B*) Monolayers deposited at 5 mN/m under nitrogen and in air, respectively. (*C* and *D*) Monolayers deposited at 30 mN/m under nitrogen and in air, respectively. The inset in panel *D* shows a monolayer prepared in nitrogen and then exposed to air for 30 min before reequilibration with nitrogen and deposition at 30 mN/m. The *z*-scale is 5 nm for images *A*, *B*, and the inset in *C* and 10 nm for images *C* and *D*.
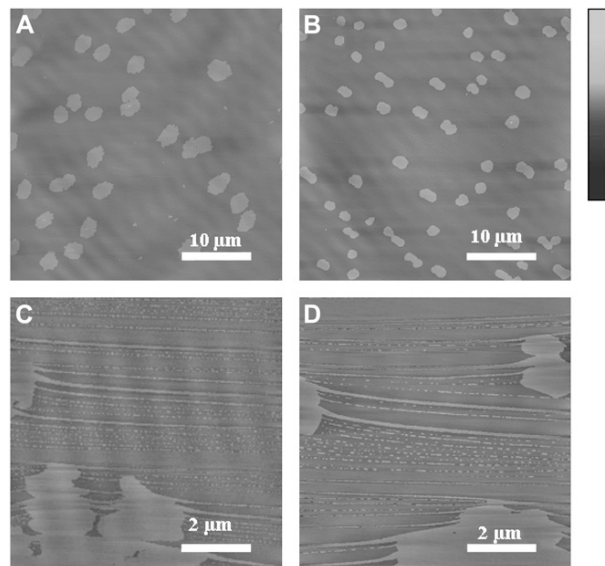

FIGURE 4 AFM images of 1:1 DOPC/DPPC monolayers transferred to mica at 10 (*A* and *B*) and 30 mN/M (*C* and *D*). Monolayers shown in Fig. 4, *A* and *C*, were deposited under nitrogen whereas those shown in Fig. 4, *B* and *D*, were deposited in air. The *z*-scale for all images is 10 nm.

large to small interconnected domains in more detail, monolayers were prepared and imaged at a series of deposition pressures (Fig. 5). AFM images of monolayers transferred at 10 mN/m showed both large domains (5–10 μm) and small islands (150–350 nm) of condensed phase (Fig. 5 A). A mixture of micro- and nanodomains was also obtained when the deposition pressure was increased to 15, 20, and 25 mN/m (Fig. 5, B–D). However, close examination of images for these monolayers indicates that there are significant changes in the sizes and numbers/surface coverage for the small and large domains with increasing pressure. Firstly, the size of the nanodomains decreases to 150–250 nm at 25 mN/m and their surface coverage increases (from 15% at 10–15 mN/m to ~30% at 20–25 mN/m). Secondly, the number of large domains decreases over the same range of pressures. For example, examination of multiple 40 × 40 μm^2 images, shows that the number of microdomains has decreased from 20 to 25 per image for monolayers transferred at 10–15 mN/m to 4–7 for monolayers deposited at 20–25 mN/m. The domains at higher pressure have more irregular edges and at

25 mN/m there are occasional areas with interconnected nanodomains that appear to originate from a larger, disrupted domain (see *inset* in Fig. 5 D). In addition to these changes, the size of the small holes containing fluid phase within the large domains increases from 40–100 nm at low pressure to 60–200 nm at 25 mN/m.

The most dramatic change in the structural organization of the membrane was obtained for monolayers transferred at 30 mN/m (Fig. 5 E). At this deposition pressure, small interconnected domains (<300 nm) distributed across the entire sample were observed. The pressure was increased even further to check for coalescence of the two phases. Although phase separation remained at 40 mN/m, the domains were even smaller in size (<250 nm) and more densely packed. The deposition pressure could not be increased further due to monolayer collapse at higher pressures. The total surface coverage of the raised domains (all sizes) increases from ~28% at low pressure to ~35% at 40 mN/m, similar to the data in Table 1 for the same mixture (but a different independently prepared set of monolayers).
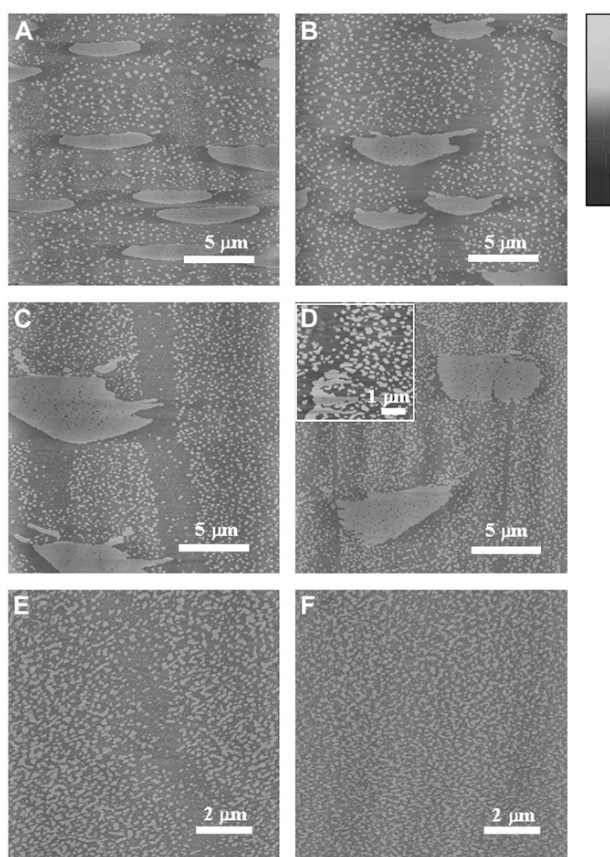
Influence of a fluorescent probe on monolayer morphology

To make a more direct comparison with earlier work that used Texas Red DHPE to visualize phase separation, we prepared monolayers of 1:1 DOPC/ESM with 20 mol % Chol and 1 mol % Texas Red DHPE under nitrogen. Both AFM topography and NSOM fluorescence for the same lipid monolayers transferred at 10 (A and B) and 30 mN/m (D and E) are shown in Fig. 6. Based on the similarity of AFM images recorded for the 1:1 DOPC/ESM and 20 mol % Chol monolayers deposited at 10 and 30 mN/m in the absence (Fig. 1, A and C) and presence of 1 mol % Texas Red DHPE (Fig. 6, A and D), we conclude that the addition of the dye-labeled lipid does not significantly alter either the morphology or size of the micrometer-sized condensed domains observed at 10 mN/m or the shape of the nanodomains and their interconnectivity in the monolayers transferred at 30 mN/m. Small variations in the size and shape of the domains between repeated control experiments are attributed to slight differences in the molar ratios of the lipid mixtures and/or to subtle changes in transfer of the monolayer from the gas-water interface to the mica support.

Previous work has shown that Texas Red DHPE is preferentially localized in the fluid phase of DOPC/brain SM/Chol and brain phosphatidylcholine/brain SM/Chol monolayers (25,26). Our NSOM data confirm the results reported for monolayers deposited at low pressure and provide additional information on the membrane organization and dye partitioning on the nanoscopic scale. As can be seen in Fig. 6, A and B, there is excellent agreement between the AFM and NSOM images for monolayers transferred at 10 mN/m. The large domains observed by AFM are readily visible as dark domains in a fluorescent background in the NSOM

FIGURE 5 Effect of surface pressure on the phase behavior of monolayers of 1:1 DOPC/ESM and 20 mol % Chol. Monolayers were transferred at 10, 15, 20, 25, 30, and 40 mN/m under nitrogen (Fig. 5, A–F). The z-scale is 10 nm for all images. The inset in panel D shows an expanded view of a partially formed large domain.
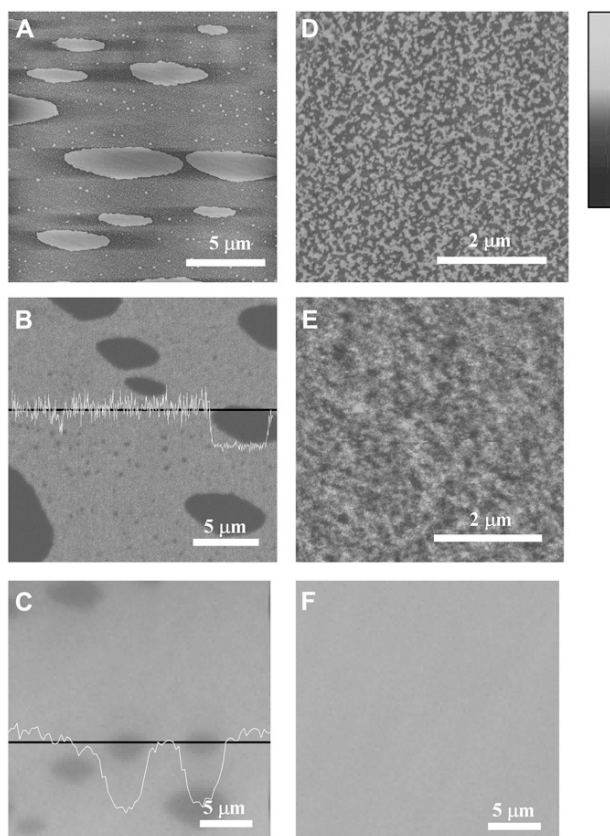
FIGURE 6 Effect of a fluorescent probe on the lateral structure of mono-layers of 1:1 DOPC/ESM with 20 mol % Chol deposited under nitrogen. Lipid monolayers containing 1% Texas Red DHPE were imaged using AFM (*A* and *D*), NSOM (*B* and *E*), and TIRFM (*C* and *F*). Images *A*, *B*, and *C* show the topography, NSOM fluorescence, and TIRFM images for a mono-layer transferred at 10 mN/m. The topography, NSOM fluorescence, and TIRFM images for a monolayer transferred at 30 mN/m are shown in Fig. 6, *D*–*F*. The z-scale for the AFM images is 5 nm.

image. Furthermore, the small islands that range in size from ~40 to 250 nm in the AFM image are also observed by NSOM. However, the larger size of the NSOM probe (esti-mated as 80–90 nm from the full width at half maximum of the point spread function of 40 nm fluorescein-labeled poly-styrene beads) means that only the larger islands can be re-solved. The fluorescent lipids partitioned sharply across the boundaries of both large domains and small islands of con-densed phase. However, the fluctuations of the optical signal, shown in the cross section in Fig. 6 *B*, were ~3–4× larger in magnitude in the fluorescent regions than in the dark domains. This indicates a heterogeneous distribution of fluorophore in the fluid phase, which we attribute to small islands of con-densed phase that are not clearly resolved in the image. For comparison, we also show the image of the same monolayer obtained by total internal reflection fluorescence microscopy (TIRFM) (Fig. 6 *C*). In this case, only the micrometer-sized domains are detected. The comparison of cross sections

showing the domain boundaries for the NSOM and TIRFM images shows the increased resolution for the NSOM image.

The NSOM image for the 1:1 DOPC/ESM monolayer with 20% Chol at 30 mN/m (Fig. 6 *E*) is heterogeneous, con-sistent with the small, interconnected domains observed by AFM (Fig. 6 *D*). In this case the domain boundaries are not well resolved since the domain separation that we measure by AFM is ~60 nm, which is similar to the aperture size of the NSOM probe used for this experiment (50–60 nm, esti-mated as described above). However, our results clearly de-monstrate the utility of NSOM to address the question of phase separation on the nanometer scale by using a fluorescent lipid to provide contrast between lipid phases. The same monolayer imaged by TIRFM appears homogeneous (Fig. 6 *F*).

Replacement of cholesterol with dihydrocholesterol

Literature studies have shown that Dchol shows similar behavior to Chol in monolayers of binary mixtures with DMPC (27) and is advantageous for minimizing oxidation since it lacks the 5,6 double bond that is the primary site of oxidative damage. Therefore, we examined the effect of replacing Chol with Dchol in the two ternary lipid mixtures for monolayers deposited at 30 mN/m under air and nitrogen. A 1:1 DOPC/DPPC monolayer containing 20% Dchol pre-pared under nitrogen showed small interconnected domains (Fig. 7 *A*) that are comparable to those obtained with Chol, thus indicating the Dchol does not change the monolayer morphology for this mixture. Monolayers for the same mix-ture prepared in air had a mixture of large and small domains (Fig. 7 *B*), indicating that the changes induced by air expo-sure do not require the presence of Chol. The height differ-ence between domains and fluid phase and the surface area covered by the domains increased slightly for a monolayer exposed to air, as observed for the ESM ternary lipid mixture (Table 1). For ternary mixtures of 1:1 ESM/DOPC with 20% Dchol, monolayers transferred under nitrogen gave both large and small domains indicating that in this case Dchol does modify the monolayer morphology, independent of any possible oxidation.
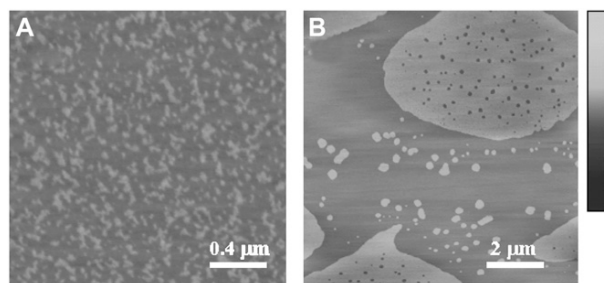

FIGURE 7 AFM images of monolayers of 1:1 DOPC/ESM with 20% mol Dchol transferred to mica at 30 mN/m under nitrogen (*A*) and air (*B*). The z-scale is 2 nm for image *A* and 5 nm for image *B*.

DISCUSSION

The AFM results obtained for monolayers of two ternary lipid mixtures demonstrate that significant differences in morphology are obtained at high surface pressure (30 mN/m) for samples deposited in air and nitrogen, in agreement with earlier fluorescence studies of similar mixtures (25,26). However, the higher spatial resolution available with AFM enables the observation of nanoscale structure that is undetectable with the diffraction-limited resolution of conventional fluorescence microscopy. This leads to two main conclusions: 1), the two ternary raft mixtures that we have examined show an evolution from mixtures of small nanodomains and larger microdomains at low surface pressure to interconnected nanodomains at high surface pressure; and 2), exposure of these monolayers to air before deposition at high surface pressure gives significant changes in morphology, with transformation of the small nanodomains into large micrometer-sized domains. These two observations are discussed separately in the following sections.

Evolution of micrometer to nanometer-sized domains with increasing surface pressure

AFM reveals that 1:1 DOPC/ESM and 1:1 DOPC/DPPC monolayers containing 20% Chol prepared under nitrogen have a mixture of nano- and micrometer-sized domains at low surface pressures that evolve to a network of small interconnected nanodomains as the surface pressure increases. The interconnected nanodomains are too small and closely spaced to be resolved by fluorescence microscopy. We have confirmed that uniform monolayers are not obtained for a number of samples made using different lipid stocks and variable conditions, indicating that the formation of nanodomains is a reproducible result and is not due to the presence of impurities or oxidized lipids (see below). Consistent with this, monolayers prepared with up to 1% Texas Red DHPE show identical AFM results to monolayers without dye. The excellent agreement between optical and topographic (NSOM and AFM) images for these samples demonstrates that the addition of dye-labeled lipid does not account for the fact that phase separation was not detected previously by fluorescence microscopy (25,26). The results also illustrate the utility of NSOM for resolving nanoscale membrane organization (40). Although AFM and fluorescence lead to the same conclusion in this study, the ability to resolve fluorescent nanodomains has significant advantages for more complex mixtures. It should also be noted that a recent study has shown that some dye-labeled lipids can have significant effects on monolayer morphology (41). In this case the addition of 1% NBD-PC resulted in significant changes in the areas, shape, and interconnectivity of nanodomains for DPPC monolayers with coexisting condensed and fluid phases.

The change of monolayer morphology with increasing surface pressure was examined in more detail for the ESM raft mixture. The evolution from a mixture of nano- and micrometer-sized domains to a closely packed network of interconnected nanodomains occurs gradually. There is an increase in the fraction of surface area covered by the small domains and a concomitant decrease in the number of large domains between 10 and 25 mN/m. At 25 mN/m the large domains are noticeably sparser with irregular perimeters and larger holes of fluid phase and there are occasional partially formed microdomains. By 30 mN/m micrometer-sized domains are completely absent from the monolayer. The observation of small nanodomains is consistent with several other AFM studies of monolayers of ternary lipid mixtures (20,30). Similarly, a transition from nanodomains to larger domains has been observed for vesicle membranes for several lipid mixtures used to mimic lipid rafts. For example, studies of DLPC/DPPC/Chol mixtures show large micrometer-sized domains at low Chol concentrations whereas at higher amounts of Chol there are much smaller nanodomains that cannot be visualized by optical microscopy but are detected by either fluorescence resonance energy transfer (FRET) or AFM (42,43). A range of raft sizes has also been reported for SM/POPC/Chol mixtures based on a time-resolved FRET study (44). The fact that nanodomains are observed using different methods and different lipid mixtures is strong evidence that the domains that we observe do not reflect effects of transfer to the mica support. Furthermore, in cases where comparisons of monolayers before and after transfer have been made, there is good agreement between the two.

A theory developed by McConnell to explain phase equilibria at the air-water interface rationalizes sizes and shapes of domains in lipid monolayers on the basis of a competition between the opposing forces of line tension and dipole densities (45). The line tension at the domain boundary favors large circular domains whereas dipolar or electrostatic interactions between molecules within domains favor small and/or extended or irregular shapes (27). Many direct determinations of rafts in giant vesicles have observed large circular domains, consistent with high line tension (13), and a variety of more complex and irregular structures have been observed as line tension is reduced by increasing the temperature (46). As noted above and summarized in several recent reviews (13,23,47) there is also considerable evidence for small raft nanodomains in many models, depending on the composition. These small features are arguably more relevant to understanding lipid organization in cellular membranes where rafts are believed to be small. However, it has been questioned whether these nanodomains correspond to thermodynamic phases and why they do not rapidly increase in size to full phase separation (13,23). A very recent report by Zimmerberg and co-workers provides a conceptual framework for understanding the factors that control domain size in phase separated mixtures (48). This study deals specifically with phase separation kinetics in flat lipid bilayers and concludes that entropic traps stabilize nanodomains in multicomponent membranes. The early nucleation and independent growth stages of phase separation occur rapidly and give nanodomains that are

typically <50 nm in radius. At longer times domain mobility and merger become important and line tension determines the domain size distribution. At low line tension, the decrease in entropy resulting from domain merger is larger than the entropy of merger and only nanodomains are present; entropy and boundary energy compete to trap nanodomains for as long as hours. Conversely, for large line tension, the decrease in boundary energy dominates the unfavorable entropy of merger and nanodomains rapidly grow to micrometer scale. At intermediate line tensions, large and small domains can coexist.

We hypothesize that a decrease in line tension with increasing surface pressure (27) accounts for the evolution of large to small domains in the raft monolayers that we have studied. The irregular shape of the nanodomains is also consistent with a relatively low line tension whereas the round or slightly elliptical domains at low pressures reflect a higher line tension. Interestingly, the mixtures of large and small domains that we observe for some mixtures/pressures are consistent with the predictions for the intermediate line tension regime based on the Zimmerberg model (48). Earlier articles by the same authors provide a detailed theoretical analysis of the dependence of the line tension on elastic moduli of the raft and the surrounding membrane (49,50). This work considers the deformations of a single monolayer that are necessary to avoid exposure of hydrophobic surfaces to water at the boundary between a thick raft and the surrounding thinner membrane and shows that lipid mixing cannot eliminate hydrophobic exposure. Calculations of the effects of lipid splay (bending) and tilt deformations show that the line tension increases quadratically with the difference in thickness between the raft and surrounding membrane. Differences in spontaneous curvature between the raft and its surroundings will reduce the line tension, in some cases to the point where rafts do not form. As shown in Table 1, the AFM data indicate a decrease (∼0.2 nm) in the height difference between raft and fluid phases when the surface pressure is increased from 10 to 30 mN/m for each of the monolayer compositions that we have examined. This variation in the height difference is presumably due to changes in packing and lipid orientation in either (or both) domains or surrounding monolayer. The model predicts that a smaller height mismatch will lead to a decrease in line tension and a concomitant decrease in raft size, exactly as observed by AFM for the two ternary lipid mixtures. Thus, our data agree qualitatively with the calculations of the effects of line tension and interaction energies on membrane rafts. Interestingly, the predictions based on this model agree well with an earlier study in which a line tension of ∼1 pN between raft and liquid-disordered domains was estimated by analyzing budding of giant unilamellar vesicles (46).

Air exposure increases the size of nanodomains

The above results indicate that preparation of monolayers in air leads to a significant increase in domain size, rather than to a change in the miscibility pressure as reported previously (25,26). However, our results are consistent with the previous hypothesis that changes in monolayer morphology are caused by oxidation of lipids at the air-water interface (25,26). The isolation of oxidized lipids from lipid monolayers exposed to air is not practical given the small amounts of material in an individual monolayer and the large number of possible products, particularly for raft mixtures in which all three components contain at least one oxidizable double bond. Despite the challenges associated with isolating oxidized materials from monolayers at the air-water interface, there is considerable evidence to support the hypothesis that lipid oxidation leads to changes in phase-separated monolayers and bilayers of unsaturated lipids, either directly by autoxidation in air or by ozone or photosensitizer (dye) mediated oxidation. In our work we have shown that the changes in monolayer morphology require the presence of air and are reproducible and irreversible. Earlier studies of similar lipid mixtures showed that air exposure led to rapid changes in surface pressure in addition to formation of large domains (25,26). Analogous surface pressure changes have been observed by ozone-mediated oxidation of POPC monolayers (28). Similarly, the addition of oxidized lipids to DPPC monolayers causes changes in the liquid-expanded to liquid-condensed transition and a concomitant increase in the amount of liquid-expanded phase, as evaluated by fluorescence microscopy (51). An earlier study showed that binary PC/Chol monolayers are also affected by exposure to air (27). This work demonstrated that a Chol oxidation product, cholestenone, is strongly line active, reducing the line tension between liquid domains in PC/Chol monolayers. This effect is identical to those observed upon exposure of monolayers to oxygen or ozone, although, of course, it does not prove that oxidation occurs (27). By contrast, other Chol oxidation products had minimal effects.

The above experimental evidence indicating that lipid oxidation alters the phase behavior of monolayers is supported by studies demonstrating that addition of oxidized lipids can promote phase separation in vesicles (52) and that autoxidation of lipids can alter Chol organization in bilayer membranes (53). Of particular relevance to our work, dye photooxidation of giant vesicles prepared from Chol/SM/DOPC mixtures resulted in the formation of large ''raft'' domains that were not observed in the absence of photooxidation (54). Although oxidized lipids were not isolated in this work, it was demonstrated that addition of a mixture of products derived from SM peroxides to giant vesicles also led to large domains, even in the absence of dye or irradiation. In parallel with our explanations, the authors conclude that the large domains are formed from nanodomains, which they detect indirectly by a fluorescence quenching assay. Based on the evidence summarized above for both monolayers and bilayers, we believe that the case for lipid oxidation promoting changes in the phase behavior of lipid membranes is compelling. Thus, we attribute our observations

of increased domain size for monolayers exposed to air to the formation of oxidized lipids that increase the line tension, thus favoring rapid formation of large domains, as predicted by the recent model (48). Interestingly the effects that we observe in monolayers occur at 30 mN/m, a pressure that is within the estimated range for modeling a biological membrane (35,36), but not at lower surface pressure (10 mN/m).

Lipid oxidation can be initiated by a variety of reactive oxygen species such as singlet oxygen, oxygen-centered radicals, or ozone and is well understood in both model and cellular membranes (55,56). The hydroperoxides formed as initial products decompose via free radical mediated lipid peroxidation that ultimately leads to a variety of products including aldehydes formed by cleavage of the alkyl chain at the site of the initial double bond. The product mixtures derived from a single lipid are complex mixtures. The range of possible products from a ternary lipid mixture in which all three lipids contain at least one oxidizable double bond plus the small amounts of material contained in individual lipid monolayers makes product isolation a formidable and impractical task. Nevertheless, the various lipid mixtures that we have examined do allow us to draw some conclusions as to which lipids are responsible for the changes in monolayer morphology. For the ternary mixtures containing DPPC, replacement of Chol with Dchol gives large domains after air exposure but not under nitrogen, indicating that Chol is not responsible for the air-induced changes, at least for this mixture. Since oxidation of the fully saturated DPPC is very unlikely, oxidized products derived from DOPC must explain the results for the DPPC/DOPC/Chol monolayers. Both ESM and DOPC are likely to contribute in the ESM ternary raft mixture. Quantitative analysis of images for the various monolayers indicates that the changes in morphology induced by air exposure for the ESM raft mixtures are accompanied by small increases in domain height and surface coverage. Both these observations and the increased line tension suggest that oxidized material is contained within the domains.

The large effects of lipid oxidation on monolayer morphology are not limited to ternary lipid mixtures with coexisting fluid and liquid-ordered phases. Of the two binary mixtures in the absence of Chol, we find that only ESM/DOPC shows a significant difference between monolayers prepared under air and nitrogen. In this case, monolayers at both high and low surface pressures show an increase in domain size in air. Since we have evidence for DOPC oxidation from the ternary lipid mixture, this result may indicate that either the binary mixtures are less readily oxidized or that the sensitivity of lipid mixtures to the presence of oxidized lipids is different.

Our observations of large domains that cover a greater fraction of the monolayer surface after air exposure are analogous to the effects of photooxidation in giant vesicles of similar lipid mixtures (54). However, we conclude that both DOPC and ESM contribute to oxidation in raft monolayers, in contrast to the bilayer results where the addition of ESM

peroxides, but not DOPC peroxides, led to the formation of large rafts. There are at least two possible explanations. As noted above, domain formation in raft mixtures may be very sensitive to the lipid composition. Alternately, variation in oxidation products between the two experiments may contribute to the differences. The situation may be further complicated by the fact that some monolayer oxidation products can be expelled to the aqueous phase, in which case changes in phase separation may be due to variation of lipid ratios rather than introduction of oxidized materials (28,29). It is also noteworthy that earlier studies of binary mixtures of DMPC and Chol showed that air exposure led to reduced line tension at a given pressure (thus reducing the pressure at which shape transitions occurred), in contrast to our results and previous reports (25,26,54) where exposure to air promoted the formation of large domains consistent with increased line tension. This raises the interesting possibility that lipid oxidation may either promote or reduce the formation of large rafts, depending on the products formed.

Summary and implications

In summary, AFM studies of monolayers of ternary lipid mixtures prepared in a nitrogen environment show a gradual evolution from a mixture of small and large domains at low surface pressures to a closely packed network of interconnected nanodomains at high surface pressure. The results are consistent with the calculated dependence of line tension on the height mismatch between the raft and the surrounding thinner monolayer, based on recent work describing the contributions of lipid bending and tilt required to avoid exposure of hydrophobic surfaces to water at the raft boundary (49,50). Exposure of monolayers to air before deposition has minimal effect at low surface pressures but leads to transformation of nanodomains to large micrometer-sized domains at high surface pressure (30 mN/m). These changes do not require the presence of Chol, as indicated by results for binary lipid mixtures and for mixtures in which Chol is replaced by Dchol. Based on our experiments and literature precedent, we assign the effects of air exposure to the generation of oxidized lipids.

These findings reinforce the importance of preparing monolayers of unsaturated lipids under conditions that minimize the potential for oxidation. In the absence of photosensitizers, the likelihood of oxidation of lipids in bilayers is expected to be much lower than for a monolayer at the air water interface. Consistent with this we do not find changes in morphology for bilayers prepared from the raft mixtures used here upon exposure to air. However, it is important to reexamine domain formation in asymmetric bilayers prepared from Langmuir monolayers of raft lipid mixtures. Although cells have significant concentrations of antioxidants to deal with oxidative stress, oxidative damage to lipids may contribute to modulation of raft size in natural membranes, as has been suggested by others (54).

Our results also illustrate the importance of applying techniques that are capable of probing domains on a range of length scales for studies of phase separation for lipid raft models. As noted in a recent review, this is particularly important for measurement of phase diagrams (47) and indicates the limitations of using fluorescence microscopy alone for such determinations. In particular, the recent comparison of monolayer and bilayer phase diagrams for DOPC/SM/Chol mixtures will require changes to include phase separation over a wider pressure range for monolayers (26). A number of studies have questioned the relevance of model systems that form nanodomains rather than the large domains typically detected by fluorescence microscopy. However, several studies, including our own work, now indicate that in some cases the large domains are an artifact induced by lipid oxidation (25,26,54). In fact model membranes with lipid compositions that favor nanodomains should be quite useful and relevant for understanding the factors that control lipid domain formation in cellular membranes.

REFERENCES

1. Brown, D. A., and E. London. 1998. Functions of lipid rafts in biological membranes. *Annu. Rev. Cell Dev. Biol.* 14:111–136.

2. Brown, D. A., and E. London. 2000. Structure and function of sphingolipid- and cholesterol-rich membrane rafts. *J. Biol. Chem.* 275:17221–17224.

3. Jacobson, K., and C. Dietrich. 1999. Looking at lipid rafts? *Trends Cell Biol.* 9:87–91.

4. Simons, K., and E. Ikonen. 1997. Functional rafts in cell membranes. *Nature.* 387:569–572.

5. Pike, L. J. 2004. Lipid rafts: heterogeneity on the high seas. *Biochem. J.* 378:281–292.

6. Munro, S. 2003. Lipid rafts: elusive or illusive. *Cell.* 115:377–388.

7. Simons, K., and W. L. Vaz. 2004. Model systems, lipid rafts and cell membranes. *Annu. Rev. Biophys. Biomol. Struct.* 33:269–295.

8. Maxfield, F. R. 2002. Plasma membrane microdomains. *Curr. Opin. Cell Biol.* 14:483–487.

9. Ipsen, J. H., O. G. Mouritsen, and M. J. Zuckermann. 1989. Theory of thermal anomalies in the specific heat of lipid bilayers containing cholesterol. *Biophys. J.* 56:661–667.

10. Ipsen, J. H., G. Karlstrom, O. G. Mouritsen, H. Wennerstrom, and M. J. Zuckermann. 1987. Phase equilibria in the phosphatidyl-choline-cholesterol system. *Biochim. Biophys. Acta.* 905:162–72.

11. Samsonov, A. V., I. Mihalyov, and F. S. Cohen. 2001. Characterization of cholesterol-sphingomyelin domains and their dynamics in bilayer membranes. *Biophys. J.* 81:1486–1500.

12. Veatch, S. L., and S. L. Keller. 2003. Separation of liquid phases in giant vesicles of ternary mixtures of phospholipids and cholesterol. *Biophys. J.* 85:3074–3083.

13. Veatch, S. L., and S. L. Keller. 2005. Seeing spots: complex phase behavior in simple membranes. *Biochim. Biophys. Acta.* 1746:172–185.

14. Dietrich, C., L. A. Bagatolli, Z. N. Volovyk, N. L. Thompson, M. Levi, K. Jacobson, and E. Gratton. 2001. Lipid rafts reconstituted in model membranes. *Biophys. J.* 80:1417–1428.

15. Dietrich, C., Z. N. Volovyk, M. Levi, N. L. Thompson, and K. Jacobson. 2001. Partitioning of Thy-1, GM1 and cross-linked phospholipid analogs into lipid rafts reconstituted in supported model membrane monolayers. *Proc. Natl. Acad. Sci. USA.* 98:10642–10647.

16. Crane, J. M., and L. K. Tamm. 2004. Role of cholesterol in the formation and nature of lipid rafts in planar and spherical model membranes. *Biophys. J.* 86:2965–2979.

17. Yuan, C., J. Furlong, P. Burgos, and L. J. Johnston. 2002. The size of lipid rafts: an atomic force microscopy study of ganglioside GM1 domains in sphingomyelin/DOPC/cholesterol membranes. *Biophys. J.* 82:2526–2535.

18. Burgos, P., C. Yuan, M.-L. Viriot, and L. J. Johnston. 2003. Two-color near-field fluorescence microscopy studies of microdomains (''rafts'') in model membranes. *Langmuir.* 19:8002–8009.

19. Milhiet, P.-E., M.-C. Giocondi, O. Baghdadi, F. Ronzon, B. Roux, and C. Le Grimellec. 2002. Spontaneous insertion and partitioning of alkaline phosphatase into model lipid rafts. *EMBO Rep.* 3:485–490.

20. Lawrence, J. C., D. E. Saslowsky, J. M. Edwardson, and R. M. Henderson. 2003. Real time analysis of the effects of cholesterol on lipid raft behavior using atomic force microscopy. *Biophys. J.* 84:1827–1832.

21. Rinia, H. A., M. M. E. Snel, J. P. J. M. van der Eerden, and B. de Kruijff. 2001. Visualizing detergent resistant domains in model membranes with atomic force microscopy. *FEBS Lett.* 501:92–96.

22. Edidin, M. 2003. The state of lipid rafts: from model membranes to cells. *Annu. Rev. Biophys. Biomol. Struct.* 32:257–283.

23. London, E. 2005. How principles of domain formation in model membranes may explain ambiguities concerning lipid raft formation in cells. *Biochim. Biophys. Acta.* 1746:203–220.

24. Milhiet, P. E., M.-C. Giocondi, and C. LeGrimellec. 2003. AFM imaging of lipid domains. *ScientificWorldJournal.* 3:59–74.

25. Stottrup, B. L., S. L. Veatch, and S. L. Keller. 2004. Nonequilibrium behavior in supported lipid membranes containing cholesterol. *Biophys. J.* 86:2942–2950.

26. Stottrup, B. L., D. S. Stevens, and S. L. Keller. 2005. Miscibility of ternary mixtures of phospholipids and cholesterol in monolayers and application to bilayer systems. *Biophys. J.* 88:269–276.

27. Benvegnu, D. J., and H. M. McConnell. 1993. Surface dipole densities in lipid monolayers. *J. Phys. Chem.* 97:6686–6691.

28. Lai, C. C., S. H. Tang, and B. J. Finlayson-Pitts. 1994. Interactions of monolayers of unsaturated phosphatidylcholines with ozone at the air-water interface. *Langmuir.* 10:4637–4644.

29. Abousalham, A., F. Fotiadu, G. Buono, and R. Verger. 2000. Surface properties of unsaturated non-oxidized and oxidized free fatty acids spread as monomolecular films at an argon/water interface. *Chem. Phys. Lipids.* 104:93–99.

30. Milhiet, P. E., C. Domec, M.-C. Giocondi, N. V. Mau, F. Heitz, and C. Le Grimellec. 2001. Domain formation in models of the renal brush border membrane outer leaflet. *Biophys. J.* 81:547–555.

31. Vie, V., N. V. Mau, E. Lesniewska, J. P. Goudonnet, F. Heitz, and C. Le Grimellec. 1998. Distribution of ganglioside GM1 between two-component, two-phase phosphatidylcholine monolayers. *Langmuir.* 14:4574–4583.

32. van Duyl, B. Y., D. Ganchev, V. Chupin, B. de Kruijff, and J. A. Killian. 2003. Sphingomyelin is much more effective than saturated phosphatidylcholine in excluding unsaturated phosphatidylcholine from domains formed with cholesterol. *FEBS Lett.* 547:101–106.

33. Giocondi, M.-C., S. Boichot, T. Plenat, and C. Le Grimellec. 2004. Structural diversity of sphingomyelin microdomains. *Ultramicroscopy.* 100:135–143.

34. Burgos, P., Z. Lu, A. Ianoul, C. Hnatovsky, M.-L. Viriot, L. J. Johnston, and R. S. Taylor. 2003. Near-field scanning optical microscopy probes: a comparison of pulled and double etched probes for fluorescence imaging of biological samples. *J. Microsc.* 211:37–47.

35. Nagle, J. F. 1976. Theory of monolayer and bilayer phase transitions: effect of headgroup interactions. *J. Membr. Biol.* 27:233–250.

36. Feng, S.-S. 1999. Interpretation of mechanochemical properties of lipid bilayer vesicles from the equation of state or pressure-area measurement of the monolayer at the air-water interface or oil-water interface. *Langmuir*. 15:998–1010.

37. Moraille, P., and A. Badia. 2002. Spatially directed protein adsorption by using a novel, nanoscale surface template. *Angew. Chem. Int. Ed. Engl*. 41:4303–4306.

38. Moraille, P., and A. Badia. 2002. Highly parallel nanoscale stripe morphology in mixed phospholipid monolayers formed by Langmuir-Blodgett transfer. *Langmuir*. 18:4414–4419.

39. Yuan, C., and L. J. Johnston. 2002. Phase evolution in cholesterol/DPPC monolayers: AFM and NSOM studies. *J. Microsc*. 205:136–146.

40. Ianoul, A., D. D. Grant, Y. Rouleau, M. Bani-Yaghoub, L. J. Johnston, and J. P. Pezacki. 2005. Imaging nanometer domains of β-adrenergic receptor complexes on the surface of cardiac myocytes. *Nat. Chem. Biol*. 1:196–202.

41. Cruz, A., L. Vazquez, M. Velez, and J. Perez-Gil. 2005. Influence of a fluorescent probe on the nanostructure of phospholipid membranes: dipalmitoylphosphatidylcholine interfacial monolayers. *Langmuir*. 21:5349–5355.

42. Tokumasu, F., A. J. Jin, G. W. Feigenson, and J. A. Dvorak. 2003. Nanoscopic lipid domain dynamics revealed by atomic force microscopy. *Biophys. J*. 84:2609–2618.

43. Feigenson, G. W., and J. T. Buboltz. 2001. Ternary phase diagram of dipalmitoyl-PC/dilauroyl-PC/cholesterol: nanoscopic domain formation driven by cholesterol. *Biophys. J*. 80:2775–2788.

44. de Almeida, R. F. M., L. M. S. Loura, A. Federov, and M. Prieto. 2005. Lipid rafts have different sizes depending on membrane composition: a time-resolved fluorescence energy transfer study. *J. Mol. Biol*. 346:1109–1120.

45. McConnell, H. M. 1991. Structures and transitions in lipid monolayers at the air-water interface. *Annu. Rev. Phys. Chem*. 42:171–195.

46. Baumgart, T., S. T. Hess, and W. W. Webb. 2003. Imaging coexisting fluid domains in biomembrane models coupling curvature and tension. *Nature*. 425:821–824.

47. Heberle, F. A., J. T. Buboltz, D. Stringer, and G. W. Feigenson. 2005. Fluorescence methods to detect phase boundaries in lipid bilayer mixtures. *Biochim. Biophys. Acta*. 1746:186–192.

48. Frolov, V. A. J., Y. A. Chizmadzhev, F. S. Cohen, and J. Zimmerberg. 2006. ''Entropic traps'' in the kinetics of phase separation in multicomponent membranes stabilize nanodomains. *Biophys. J*. 91:189–205.

49. Kuzmin, P. I., S. A. Akimov, Y. A. Chizmadzhev, J. Zimmerberg, and F. S. Cohen. 2005. Line tension and interaction energies of membrane rafts calculated from lipid splay and tilt. *Biophys. J*. 88:1120–1133.

50. Akimov, S. A., P. I. Kuzmin, J. Zimmerberg, F. S. Cohen, and Y. A. Chizmadzhev. 2004. An elastic theory for line tension at a boundary separating two lipid monolayer regions of different thickness. *J. Electroanal. Chem*. 564:13–18.

51. Sabatini, K., J.-P. Mattila, F. M. Megli, and P. K. J. Kinuunen. 2006. Characterization of two oxidatively modified phospholipids in mixed monolayers with DPPC. *Biophys. J*. 90:4488–4499.

52. Megli, F. M., L. Russo, and K. Sabatini. 2005. Oxidized phospholipids induce phase separation in lipid vesicles. *FEBS Lett*. 579:4577–4584.

53. Jacob, R. F., and R. P. Mason. 2005. Lipid peroxidation induces cholesterol domain formation in model membranes. *J. Biol. Chem*. 280:39380–39387.

54. Ayuyan, A. G., and F. S. Cohen. 2006. Lipid peroxides promote large rafts: effects of excitation of probes by fluorescence microscopy and electrochemical reactions during vesicle formation. *Biophys. J*. 91:2172–2183.

55. Halliwell, B., and J. M. C. Gutteridge. 1985. Free Radical in Biology and Medicine. Oxford University Press, New York.

56. Girotti, A. W. 1998. Lipid hydroperoxide generation, turnover, and effector action in biological systems. *J. Lipid Res*. 39:1529–1541.